REPORT DOCUMENTATION PAGE

Form Approved
OMB No. 0704-0188

1. REPORT DATE *(DD-MM-YYYY)*	**2. REPORT TYPE**	**3. DATES COVERED** *(From - To)*
05-10-2013		

4. TITLE AND SUBTITLE

Isolation of Thermal and Strain Responses in Composites Using Embedded Fiber Bragg Grating Temperature Sensors

5a. CONTRACT NUMBER

5b. GRANT NUMBER

5c. PROGRAM ELEMENT NUMBER

6. AUTHOR(S)
Elam, Kyle Aspie

5d. PROJECT NUMBER

5e. TASK NUMBER

5f. WORK UNIT NUMBER

7. PERFORMING ORGANIZATION NAME(S) AND ADDRESS(ES)

8. PERFORMING ORGANIZATION REPORT NUMBER

9. SPONSORING / MONITORING AGENCY NAME(S) AND ADDRESS(ES)
U.S. Naval Academy
Annapolis, MD 21402

10. SPONSOR/MONITOR'S ACRONYM(S)

11. SPONSOR/MONITOR'S REPORT NUMBER(S)
Trident Scholar Report no. 412 (2013)

12. DISTRIBUTION / AVAILABILITY STATEMENT

This document has been approved for public release; its distribution is UNLIMITED.

13. SUPPLEMENTARY NOTES

14. ABSTRACT

In this research, fiber Bragg grating (FBG) optical temperature sensors are used for structural health monitoring of composite materials. The specific goal is to detect the thermal response of a composite to high energy radiation incident on the surface of a composite structure. FBG sensors also respond to axial strain in the optical fiber, thus any structural strain experienced by the composite is also detected. Consequently, this research has focused both on identifying the unique characteristics of each response and on developing feasible methods to isolate the thermal response from the strain response. Isolation ensures that any response to mechanical strain does not mask the response to a temperature gradient present on the composite surface. The isolation strategy developed in this research is characterized by two design features. First, a three-dimensional array of FBG temperature sensors has been embedded in a carbon/epoxy composite structure, consisting of both in-plane and through-thickness sensor arrays. This architectural design component exploits the spatial differences between the temperature profile and the strain profile in a composite structure. Second, an accompanying data processing scheme has been developed that uses the statistical properties of the collected sensor data to interpret and identify each response. The degree to which the isolation strategy increases the functionality of FBG temperature sensors in mechanically strained composite structures is assessed.

15. SUBJECT TERMS

fiber Bragg grating, composites, temperature gradient, strain, data processing, structural health monitoring

16. SECURITY CLASSIFICATION OF:			**17. LIMITATION OF ABSTRACT**	**18. NUMBER OF PAGES**	**19a. NAME OF RESPONSIBLE PERSON**
a. REPORT	**b. ABSTRACT**	**c. THIS PAGE**		33	**19b. TELEPHONE NUMBER** *(include area code)*

U.S.N.A. --- Trident Scholar project report; no. 412 (2013)

ISOLATION OF THERMAL AND STRAIN RESPONSES IN COMPOSITES USING EMBEDDED FIBER BRAGG GRATING TEMPERATURE SENSORS

by

Midshipman 1/C Kyle A. Elam
United States Naval Academy
Annapolis, Maryland

_____
(signature)

Certification of Advisers Approval

Associate Professor R. Brian Jenkins
Electrical and Computer Engineering Department

_____
(signature)

_____
(date)

Associate Professor Peter J. Joyce
Mechanical Engineering Department

_____
(signature)

_____
(date)

Associate Professor Deborah M. Mechtel
Electrical and Computer Engineering Department

_____
(signature)

_____
(date)

Acceptance for the Trident Scholar Committee

Professor Maria J. Schroeder
Associate Director of Midshipman Research

_____
(signature)

_____
(date)

ABSTRACT

In this research, fiber Bragg grating (FBG) optical temperature sensors are used for structural health monitoring of composite materials. The specific goal is to detect the thermal response of a composite to high energy radiation incident on the surface of a composite structure. The unique optical characteristics of FBG sensors permit rapid detection of highly localized temperature gradients in a host structure, making FBGs well-suited for this application.

FBG sensors also respond to axial strain in the optical fiber, thus any structural strain experienced by the composite is also detected. Therefore the embedded FBG sensors respond to the mechanical strain in addition to any thermal effects. Consequently, this research has focused both on identifying the unique characteristics of each response and on developing feasible methods to isolate the thermal response from the strain response. Isolation ensures that any response to mechanical strain does not mask the response to a temperature gradient present on the composite surface.

The isolation strategy developed in this research is characterized by two design features. First, a three-dimensional array of FBG temperature sensors has been embedded in a carbon/epoxy composite structure, consisting of both in-plane and through-thickness sensor arrays. This architectural design component exploits the spatial differences between the temperature profile and the strain profile in a composite structure. Second, an accompanying data processing scheme has been developed that uses the statistical properties of the collected sensor data to interpret and identify each response. Both design features are presented here, and the degree to which the isolation strategy increases the functionality of FBG temperature sensors in mechanically strained composite structures is assessed.

Keywords: fiber Bragg grating, composites, temperature gradient, strain, data processing, structural health monitoring

ACKNOWLEDGMENTS

To begin, special thanks must be given to the faculty research advisers for this project. Dr. Brian Jenkins, Dr. Peter Joyce, and Dr. Deborah Mechtel were invaluable throughout the research process. Their guidance paved the way for the success of this research project. Additionally, the Trident and Bowman Scholar Programs Committees have been instrumental in facilitating this project. Many thanks are also warranted to the Joint Technology Office (especially Quentin Saulter and Don Seeley) and the Office of Naval Research (especially Quentin Saulter, Sarwat Chappel, and Dr. Lew DeSandre) for their generous funding of the United States Naval Academy (USNA) Directed Energy Research Center, under CAPT Richard Watkins, USN. CAPT Watkins's support for and aid in this research cannot be overstated.

The author would also like to acknowledge Cort Lillard for his assistance with the infrared laser testbed. As well, the USNA Lab Technicians provided significant technical support for this project. Lastly, special acknowledgment must be given to Dr. Robert Cozzens, Mr. Matt Evans, and Mr. Jesse Duncan, from the Naval Research Laboratory for their assistance with composite production through the course of this research.

TABLE OF CONTENTS

1. INTRODUCTION

Embedded optical sensors have several advantages over alternative electromechanical systems for structural health monitoring (SHM). While electromechanical "smart" sensors are of limited use in environments prone to electromagnetic interference (EMI), infrared optical networks are effectively immune to EMI.[1] Perhaps more pertinent to this research, the ability to multiplex optical signals on different wavelengths allows several sensors to be present in a single optical fiber. Whereas thermocouples and strain gauges require two copper leads per device, one optical fiber can contain many distinct sensors.

Optical fiber Bragg gratings (FBGs), in particular, are highly sensitive to both temperature and strain. This dual response is a potential problem for widespread application of embedded FBGs; if both thermal effects and mechanical strain are present, one response may mask the other. Accordingly, FBGs are often employed as temperature sensors in environments isolated from excessive mechanical strain[2] or as strain sensors in environments insulated from excessive thermal effects.[3]-[4] However, effective FBG use in SHM applications cannot be so limited.

The goal of this research was to embed FBG temperature sensors in composite structures, and to successfully detect a localized thermal gradient in the presence of mechanical strain. The strategy to isolate the thermal and strain responses of embedded FBG sensors had two aspects. First, an architectural design component used a three-dimensional FBG array embedded in a two-ply carbon/epoxy composite structure. This sensor array was designed such that thermal responses were distinct and identifiable compared with strain responses. Second, a data processing algorithm supplemented the architectural component. The algorithm used a statistical analysis of the sensor data to detect any potential localized thermal gradients.

2. THEORY

2.1 Fundamental FBG Characteristics

Physically, a fiber Bragg grating is a sinusoidal variation of the core index of refraction in the longitudinal direction of a fused silica optical fiber (see Figure 1). When broadband light propagating in an optical fiber is incident on an FBG, a narrow band of wavelengths reflects back toward the source. This reflection spectrum is typically narrowband and centered around the Bragg wavelength, λ_B, of the FBG. The Bragg wavelength is dependent on the physical geometry of the grating and the optical parameters of the silica core. Ideally, other wavelengths are completely transmitted through the grating.

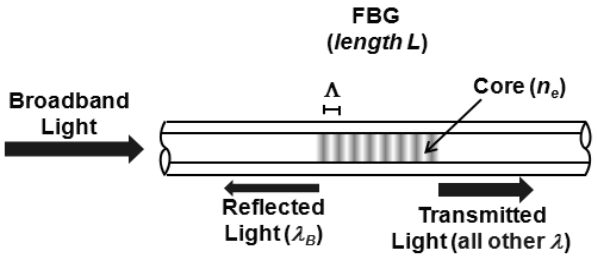

Figure 1: Longitudinal profile of a conventional FBG, where L is the grating length, n_e is the effective index of refraction of the fiber core, Λ is the spatial period, and λ_B is the Bragg wavelength.

Quantitatively, the Bragg wavelength depends on the effective index of refraction of the fiber core n_e and the spatial period of the grating's sinusoidal index variation Λ, as described by:

$$\lambda_B = 2n_e\Lambda\,. \tag{1}$$

In optical communications, FBGs are often used as narrow-band filters or to perform wavelength division multiplexing (WDM) or demultiplexing of information on different optical frequencies. To use FBGs in sensor

applications, however, the FBG response to physical stimuli must be characterized. The Bragg wavelength is highly dependent on both the grating temperature and mechanical strain in the optical fiber. Differentiating Equation (1) with respect to both T (temperature) and ε (strain) gives

$$\frac{\partial \lambda_B}{\partial T} = 2n_e \frac{\partial \Lambda}{\partial T} + 2\Lambda \frac{\partial n_e}{\partial T}, \tag{2}$$

$$\frac{\partial \lambda_B}{\partial \varepsilon} = 2n_e \frac{\partial \Lambda}{\partial \varepsilon} + 2\Lambda \frac{\partial n_e}{\partial \varepsilon}. \tag{3}$$

Some simplifying assumptions are helpful to distinguish the temperature and strain dependence of λ_B. The temperature dependence of the Bragg wavelength is primarily a function of the thermo-optic properties of the fused silica glass. Because silica glass has a low coefficient of thermal expansion, the variation in n_e with respect to T is much larger than the variation in Λ. Hence, the second term in Equation (2) is dominant. In contrast, the variation in Λ due to strain ε (elongation or contraction) is considerably larger than the variation in n_e, so the first term in Equation (3) primarily determines the shift in λ_B due to strain.[1] Thus, the thermal FBG response is primarily due to the temperature dependence of n_e while the strain response depends primarily on variation in the value of Λ.

Based on these practical assumptions, Equations (2) and (3) are more simply stated as:

$$\frac{\partial \lambda_B}{\partial T} = 2\Lambda \frac{\partial n_e}{\partial T}, \tag{4}$$

$$\frac{\partial \lambda_B}{\partial \varepsilon} = 2n_e \frac{\partial \Lambda}{\partial \varepsilon}. \tag{5}$$

For common operating temperatures and typical loading conditions, a shift in Bragg wavelength $\Delta\lambda_B$ is linear with respect to shifts in temperature ΔT and strain $\Delta\varepsilon$, so that Equations (4) and (5) can be written as

$$\frac{\Delta \lambda_B}{\Delta T} = 2\Lambda \frac{\Delta n_e}{\Delta T} = 10.3 \ \frac{\text{pm}}{\text{°C}}, \tag{6}$$

$$\frac{\Delta \lambda_B}{\Delta \varepsilon} = 2n_e \frac{\Delta \Lambda}{\Delta \varepsilon} = 1.2 \ \frac{\text{pm}}{\mu\varepsilon}. \tag{7}$$

The sensitivity values in (6) and (7) are typical for FBGs written in silica glass fiber with Bragg wavelengths near 1550 nm.[1] The sensitivity values are different in plastic fibers or metal-clad fibers, for example.

2.2 Thermal Effects on FBGs

Qualitatively, Equation (6) describes the temperature dependence of the Bragg wavelength. An increase in the effective refractive index due to temperature causes an increase in the Bragg wavelength. Figure 2 illustrates this effect with and without heat applied to the sensor. As stated in Equation (6), the constant of proportionality (or sensitivity) for such a shift is 10.3 pm/°C. The thermal sensitivity is itself dependent on other environmental factors, so its value must be precisely calibrated for high-accuracy temperature measurements.[5]

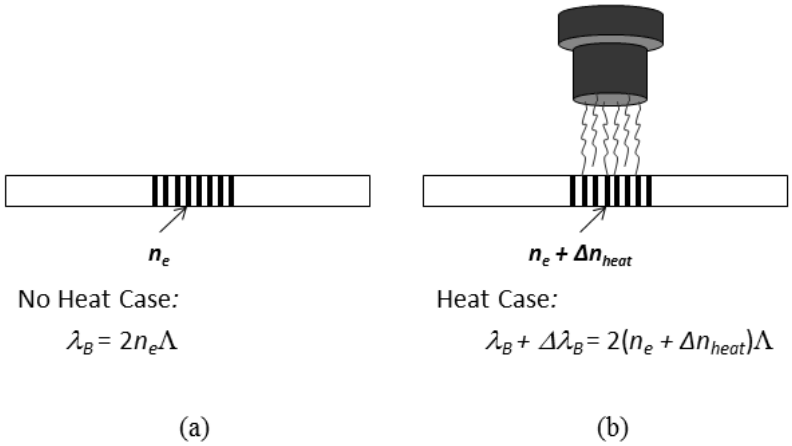

Figure 2: Diagrams show the effect of heat on the Bragg wavelength. (a) With no heat applied, λ_B follows Equation (1) as expected. (b) If the FBG is exposed to a heat source (i.e. a heat gun), then λ_B experiences a positive shift of $\Delta\lambda_B$.

2.3 Strain Effects on FBGs

Equation (7) describes how strain affects the Bragg wavelength. A change in the grating period due to compression or tension causes a proportional change in the Bragg wavelength equal to 1.2 pm/με. Figure 3 illustrates this effect for two cases: no strain and tension/compression.

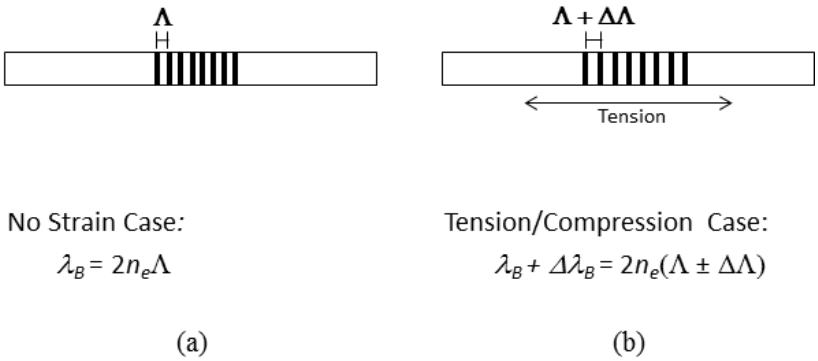

Figure 3: Diagrams showing the effect of strain on the Bragg wavelength. (a) When no strain is applied, λ_B follows Equation (1). (b) When strain is applied to the fiber, λ_B experiences a shift of $\Delta\lambda_B$. In the figure, tensile strain is applied, elongating the grating and causing a positive shift in the Bragg wavelength. Alternatively, if compressive strain is applied, the grating experiences a downshift in the Bragg wavelength.

2.4 FBG Interrogation

To monitor shifts in the Bragg wavelength of an FBG, an interrogation scheme is required. Various techniques can be used to interrogate an FBG sensor. The most common uses a tunable laser or broadband source to scan through the wavelength band to be interrogated. The signal reflected from the FBG is separated from the transmitted signal using a circulator between the tunable laser and the sensors. A power sensor is used to monitor the reflected optical power. Data acquisition software in the interrogator determines the peak reflected power level that corresponds to the Bragg wavelength. This process is illustrated in Figure 4.

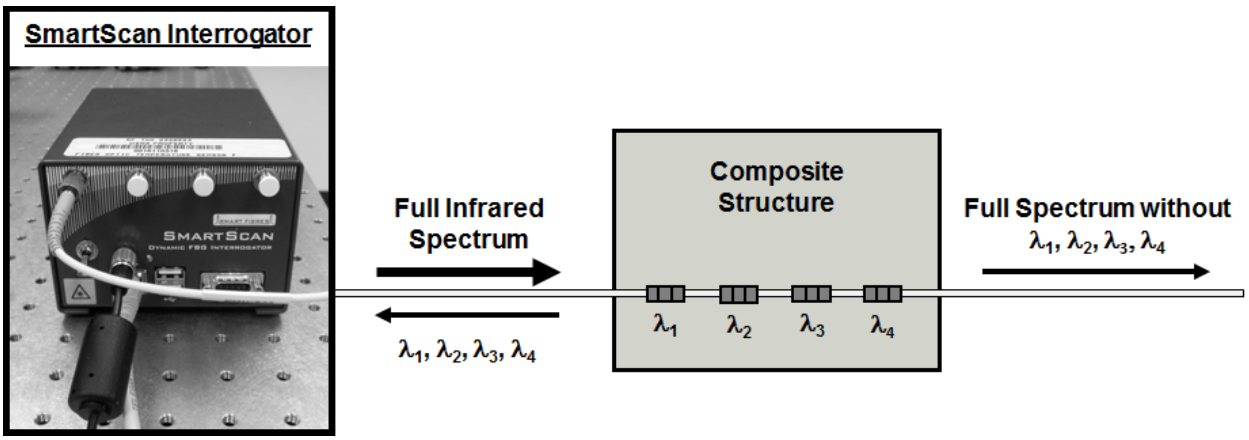

Figure 4: Smart Fibres© SmartScan Interrogator is used to track the Bragg wavelengths of four FBG sensors.

Two interrogator options were available for this project. High spectral resolution using a single scan with wavelength intervals as small as ~10pm could be achieved using standard optical components (i.e. tunable lasers, circulators, power sensors) already present in the lab. To further improve the spectral resolution, interpolative peak-detection techniques were sometimes applied to the collected data. For more rapid, dynamic scans, a Smart Fibres© SmartScan high speed interrogator was also available that can scan the spectrum between 1525 nm and 1565 nm on four separate input channels at rates up to 2.5 kHz per channel. The spectral resolution was reduced when scanning at higher rates. In this research, most of the thermal and strain responses required a dynamic scan, so the SmartScan interrogator was primarily used.

3. STRUCTURAL ISOLATION METHODOLOGY

To use embedded FBGs as temperature sensors in a composite structure, it is necessary to isolate the thermal response of the sensors from the strain response. There are two features of the overall isolation strategy pursued in this research. First, FBG sensor fibers are embedded in an architectural arrangement that ensures the FBG responses due to strain are predictable (i.e. deterministic). Second, the responses from the sensors are then processed using an isolation algorithm written in MATLAB®. The data processing algorithm uses the sensor response data to determine if a localized thermal gradient is present in the composite structure.

3.1 Through-Thickness FBG Array Design

Ignoring torsion and other higher-order effects, the simplest strain experienced in a long, wide, and thin structure (i.e. a wing) results from bending. When such a structure bends, one face experiences compression and the other face experiences tension. One method to isolate a thermal response from a strain response uses an array of FBGs embedded through the thickness of the structure, as shown in Figure 5. The shift in Bragg wavelength for each grating varies depending on its depth in the structure. For example, in Figure 5, the Bragg wavelength λ_B of the top-layer FBG shifts to a higher value to indicate tension. The FBG in the middle experiences no shift in λ_B because it is located along the strain-neutral axis. Lastly, the bottom-layer FBG shifts to a lower λ_B value due to compression.

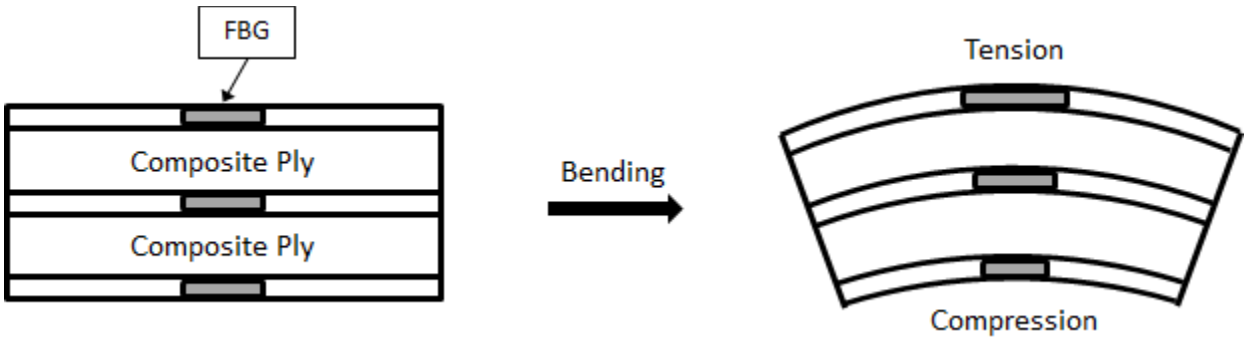

Figure 5: Through-thickness FBG array experiences symmetric strain on both faces during bending. The inner face experiences compression and the outer face experiences tension. The centrally located FBG is located along the strain-neutral axis and experiences no strain effects.

Without thermal effects, the response of the top- and bottom-layer FBGs are symmetric about the neutral axis. However, if an FBG on one face experiences a temperature-based upshift in Bragg wavelength, the FBG response through thickness becomes asymmetric. To detect thermal gradients using this method, the interrogation system must monitor the degree of symmetry found in the through-thickness FBG array. Asymmetric through-thickness responses indicate the presence of localized thermal gradients on one surface. This method requires thicker structures with sufficient thermal mass to insulate thermal effects between the opposing faces.

3.2 In-Plane FBG Array Design

Another method to isolate a thermal response from a strain response using multiple sensors in an FBG array is to orient the sensors so that they all experience similar mechanical strain. Changes in the response of individual gratings in such an array would indicate the presence of a localized thermal gradient. Since FBGs responds to axial strain in the host fiber, all sensor fibers should be oriented parallel to each other. This requires a planar array of parallel fibers that run through the length of the structure. An example is the in-plane *n* x *m* sensor array illustrated in Figure 6. There are *n* sensor fibers in the array, each with *m* FBG sensors per fiber.

By embedding parallel sensor fibers within or below the surface of a composite structure, bending induces a similar response in each grating in the array. Since all FBGs are embedded at the same depth in the structure, all FBGs in the array uniformly experience either tension or compression. If a localized thermal gradient is also present, this uniformity is lost. Thus, a non-uniform response from an in-plane FBG array indicates the presence of thermal gradients in the structure.

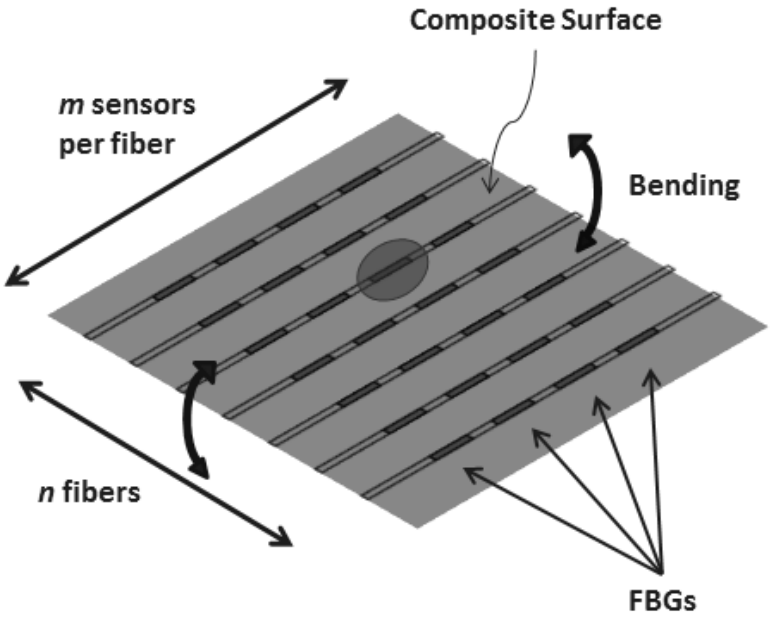

Figure 6: An *n* x *m* in-plane FBG array embedded in a composite structure. Ideally, all gratings experience uniform axial strain. If an FBG experiences a localized thermal gradient (shown as the shaded area above), this uniformity is lost and the thermal gradient has been detected.

3.3 Three-Dimensional FBG Array Design

A three-dimensional FBG array embedded in the plane of a composite and through its thickness can be used to perform a comprehensive analysis of thermal and strain effects. To explore this methodology, a 3x2x2 test array of FBGs was embedded in a two-ply carbon/epoxy composite structure, as shown below in Figure 7. The nominal Bragg wavelength is shown adjacent to each FBG (λ_B is given in nm).

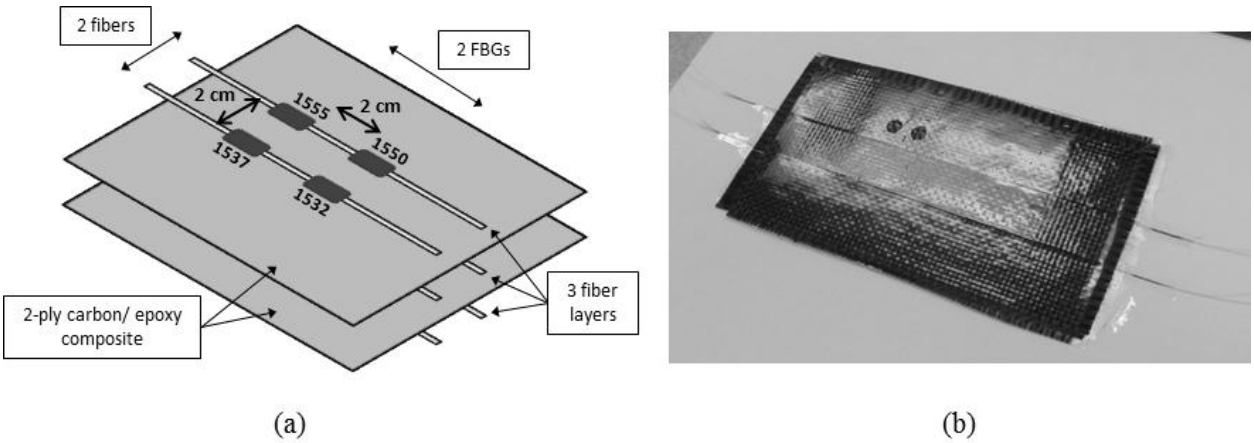

Figure 7: A three-dimensional 3x2x2 FBG array. (a) Sensor fibers and FBGs are indicated. There are three layers of 2x2 in-plane FBG arrays interleaved above, between, and below two plies of carbon fiber weave. Each FBG is approximately 1 cm in length. (b) A photograph of the embedded FBG array.

To interrogate the six sensor fibers of the test array with the four available input channels on the SmartScan interrogator, wavelength division multiplexing (WDM) is used. Functionally, WDM is a combination of multiple optical signals that each occupy separate wavelength bands. Figure 8 illustrates the interrogation architecture using a WDM device. The interrogator transmits a broadband infrared signal between 1525 nm and 1565 nm. This signal

is split (demultiplexed) by the WDM device, which is manufactured to operate in two specific wavelength bands. Wavelengths between 1547-1561 nm propagate from the upper port of the WDM device in Figure 8 to the upper fiber in the composite. Signals between 1529-1542 nm propagate from the lower port. For each fiber in the composite, reflections occur in a narrow spectral window at the Bragg wavelengths of each FBG. The reflected signals are recombined (multiplexed) by the WDM device and return to the interrogator. Using this WDM scheme, each interrogator input channel monitors two sensor fibers. This scheme is replicated for each of the three fiber layers of the 3x2x2 FBG array, using three of the SmartScan interrogator input channels.

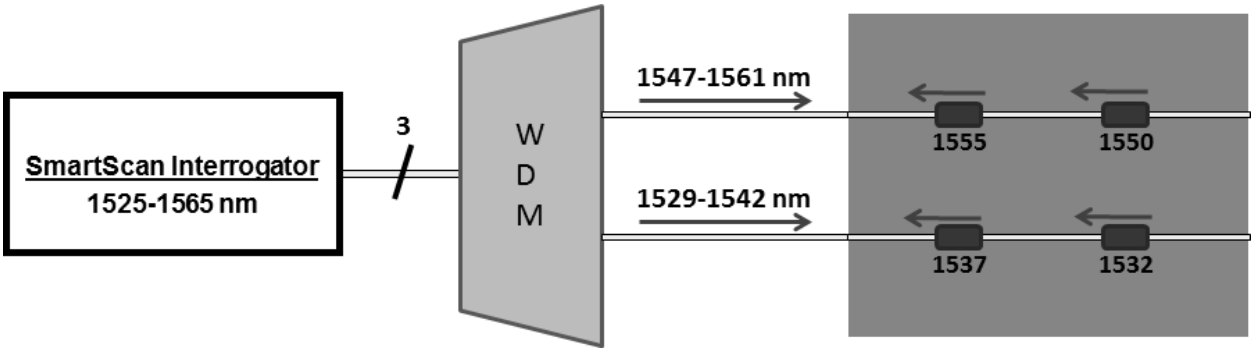

Figure 8: WDM scheme used to interrogate a 3x2x2 FBG array. Nominal Bragg wavelengths of the gratings are given in nm.

4. COMBINED THERMAL AND STRAIN TESTING

After initial testing on simpler composite structures to investigate thermal and strain responses of embedded FBGs, combined thermal and strain tests were conducted with the 3x2x2 test array. The goal of these tests was to validate the structural isolation techniques described above.

4.1 Nondestructive Test Setup

For nondestructive testing of the sample, a conventional heat gun was used to produce localized temperature shifts of 100°C or slightly higher in the material. Thermal effects on this scale are not significant enough to permanently damage the composite structure containing the 3x2x2 test array. However, the thin composite samples used in this research did experience some warping when exposed to the heat gun for long time periods. The heat gun provided a convenient benchtop heat source, but it cannot produce highly localized thermal energy on the face of the composite. For example, when the heat gun was directed at only one specific grating in the FBG array, thermal effects were exhibited by all gratings in the plane of the composite, as shown in Figure 9. However, the heat gun was useful for initial nondestructive testing.

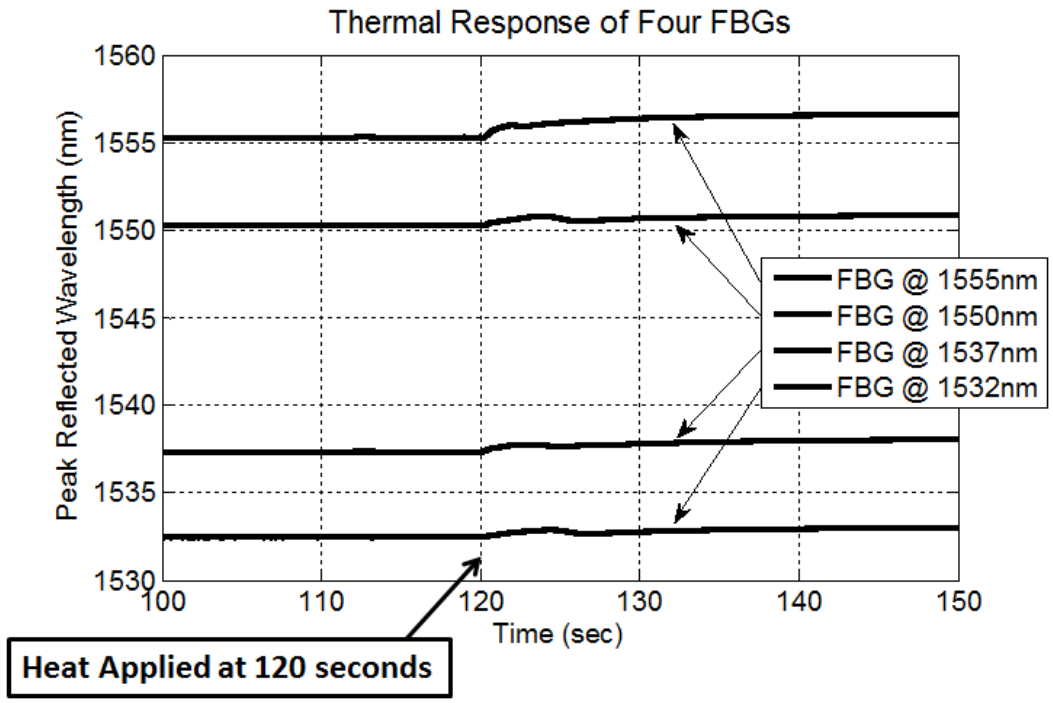

Figure 9: Thermal response of the four FBGs embedded in the front plane of the 3x2x2 array. A heat gun directed at the 1555 nm sensor was turned on at 120 seconds. The FBG sensors all respond with an upshift in the corresponding Bragg wavelengths.

To induce controlled oscillatory strain in the composite sample, a cyclic strain apparatus was constructed. The apparatus used a 24 Volt DC electric motor geared to achieve a maximum of 109 RPM at full voltage. A circular aluminum disc was attached to the end of the motor's axle. By offsetting the axle from the center of the disc, a rotation of the disc about the axle while in contact with the composite structure deflected the structure a known amount. As the motor rotated cyclically, the composite experienced a repeatable, cyclic deflection. For this research, the disc was designed to create a 1.3 cm deflection with every rotation. Figure 10 shows a top view diagram and a side view photograph. Figure 11 illustrates the through-thickness strain response of three sensors when the cyclic strain apparatus is used to deflect the 3x2x2 test array. Figure 12 shows a combined thermal/strain setup with the heat gun and the cyclic strain apparatus.

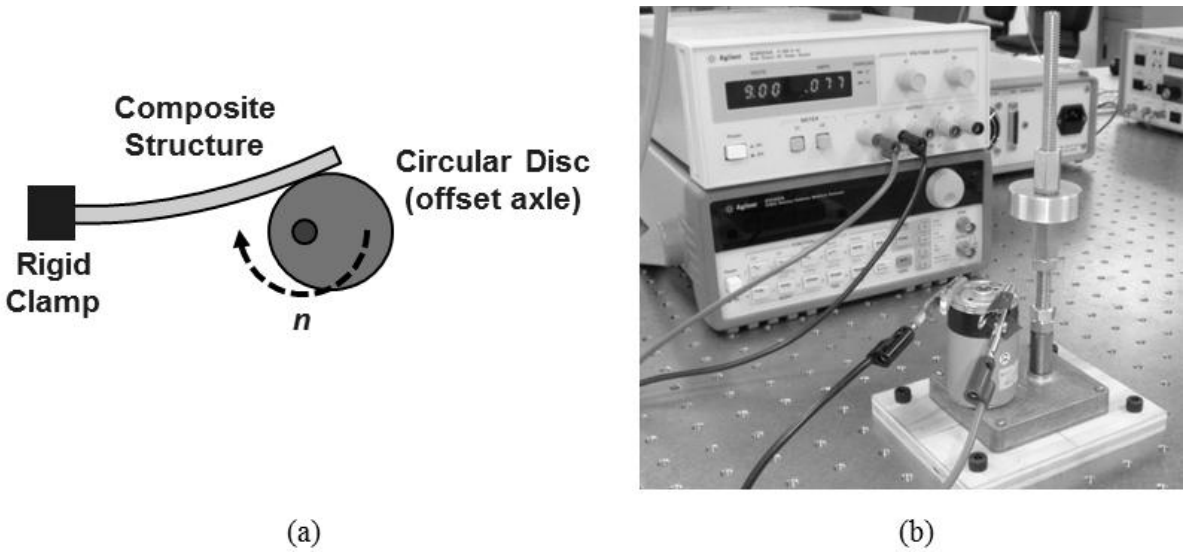

Figure 10: (a) Top view of the cyclic strain apparatus in contact with a rigidly clamped composite structure. As the disc rotates, the structure deflects accordingly. (b) Side view of the cyclic strain apparatus (foreground) with a DC voltage source (background) to provide the desired drive voltage. Here, 9.00 Volts DC are applied.

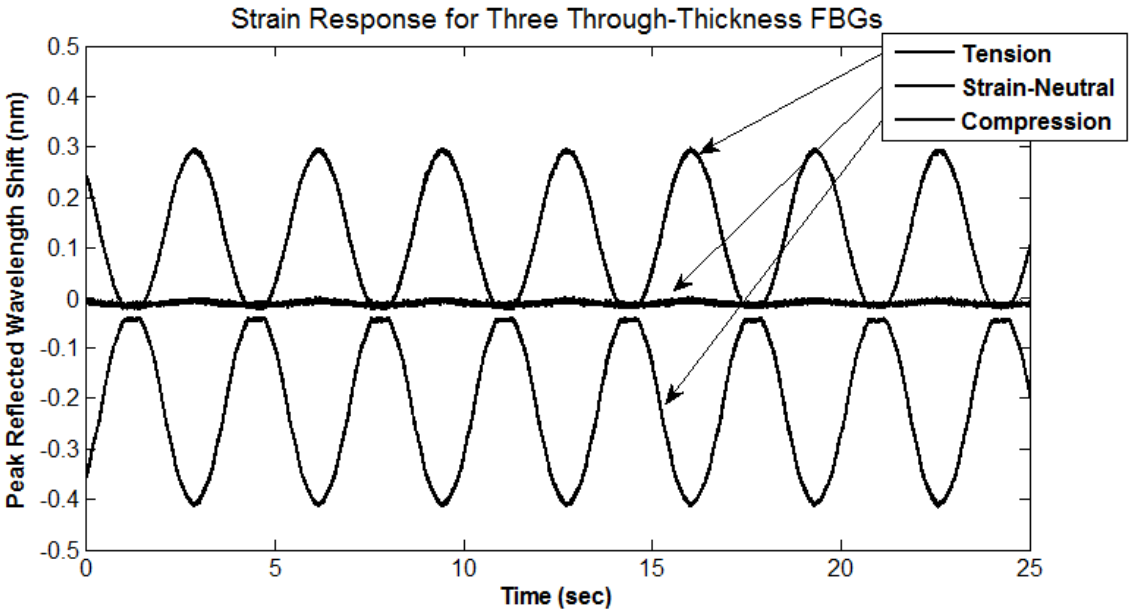

Figure 11: Through-thickness strain response of FBGs when cyclic strain is applied to the host structure. Through the thickness, one FBG sensor responds to cyclic tension, the middle layer sensor experiences minimal strain on the strain-neutral axis, and the last FBG sensor responds to cyclic compression.

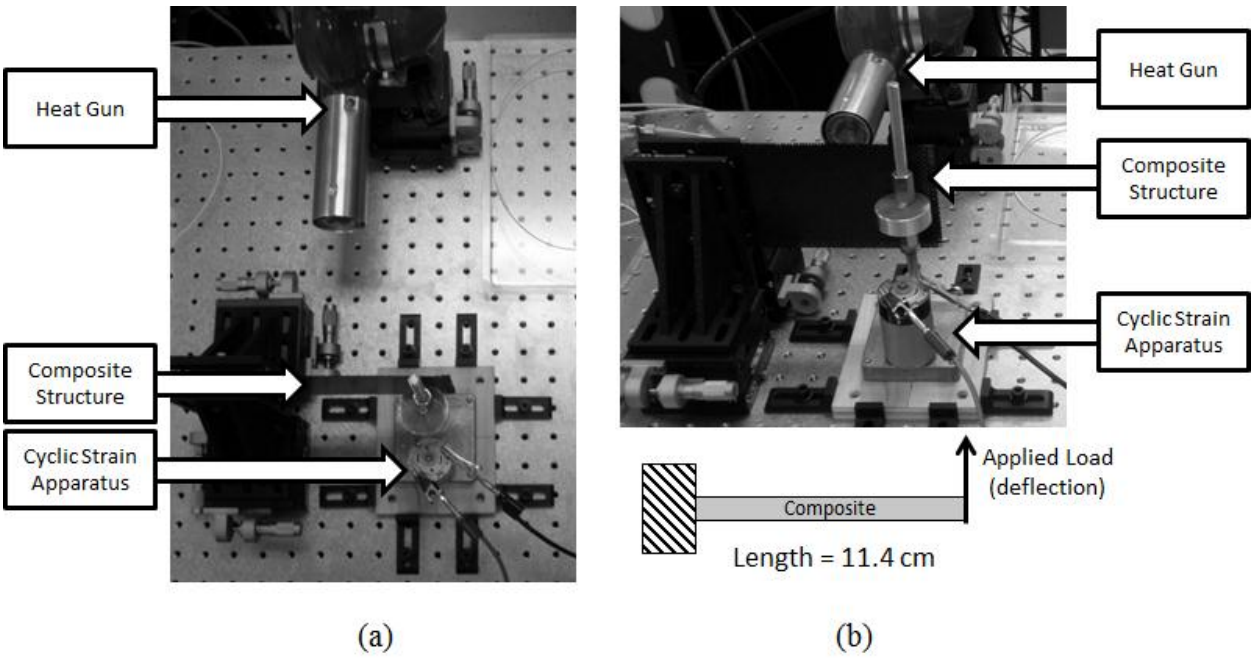

Figure 12: (a) Top view of combined thermal and strain test setup. A conventional heat gun applies heat and the cyclic strain apparatus applies cyclic strain. (b) Side view of the same test setup, with a free body diagram of the composite with the load.

4.2 Infrared Laser Test Setup

As noted above, a heat gun is not necessarily effective as a localized heat source, so an alternative source was needed to generate a highly localized thermal gradient on the surface of the composite. A 1070-nm infrared laser was used that generated 25 W of optical power focused onto a 5 mm diameter spot size. The laser can generate a maximum possible power of 100 W in a 5 mm spot, giving a maximum irradiance of 500 W/cm^2. At these higher optical power levels, the composite can suffer permanent damage depending on the length of time the laser is incident on the composite surface. The thermal conductivity of the carbon/epoxy composite was too small to dissipate the large, rapid deposit of thermal energy. As a result, the laser bored a hole through the thin two-ply structure after roughly 20 seconds. In these tests, laser energy was applied to the composite with the embedded 3x2x2 FBG array for 20 seconds at two target locations, as shown in Figure 13. To avoid permanent damage to the 1555 nm FBG sensor, the laser was not aimed directly at the grating. Instead, the target locations were at least 1.0 cm away, preserving all of the FBGs for additional tests. The testing conditions described here intentionally limited the thermal effects produced by the laser to ensure useful data collection without causing permanent damage to the FBGs.

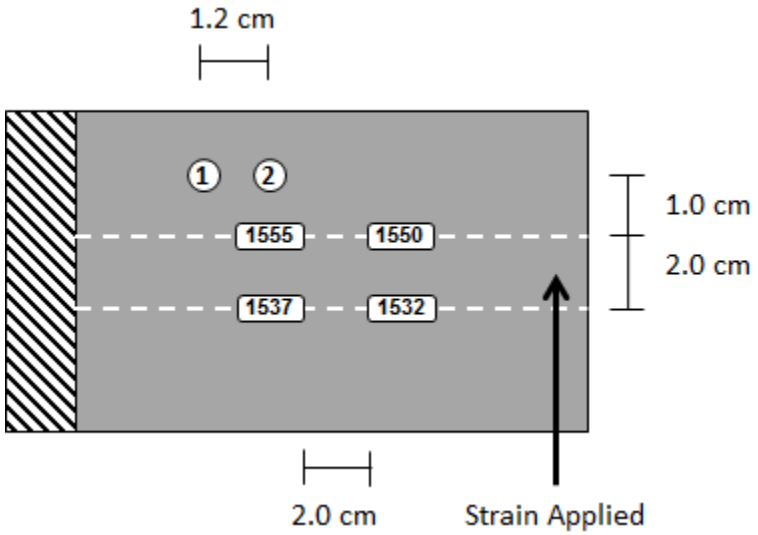

Figure 13: Infrared laser target locations 1 and 2 displayed with dimensions on the 3x2x2 FBG array (side view as seen in Figure 12(b)). The left end of the composite is firmly clamped. Strain is applied to the right side. Figure not to scale. All nominal Bragg wavelengths are given in nm.

With this higher energy heat source, several precautions are taken. First, a steady flow of high-velocity nitrogen gas is blown over the front face of the composite, extinguishing flames that result from the laser energy. Second, a vacuum is placed above the composite structure, removing smoke, ash, and other debris created during the lasing process. The high-velocity nitrogen flow and the vacuum ensure that the composite surface is clean and free of soot and debris, and that the majority of the incident optical energy is absorbed directly into the composite structure, creating a well-defined and localized temperature gradient. The complete test chamber setup is shown in Figure 14. The cyclic strain apparatus shown in Figure 14 was used to induce a 0.3 Hz oscillatory mechanical strain.

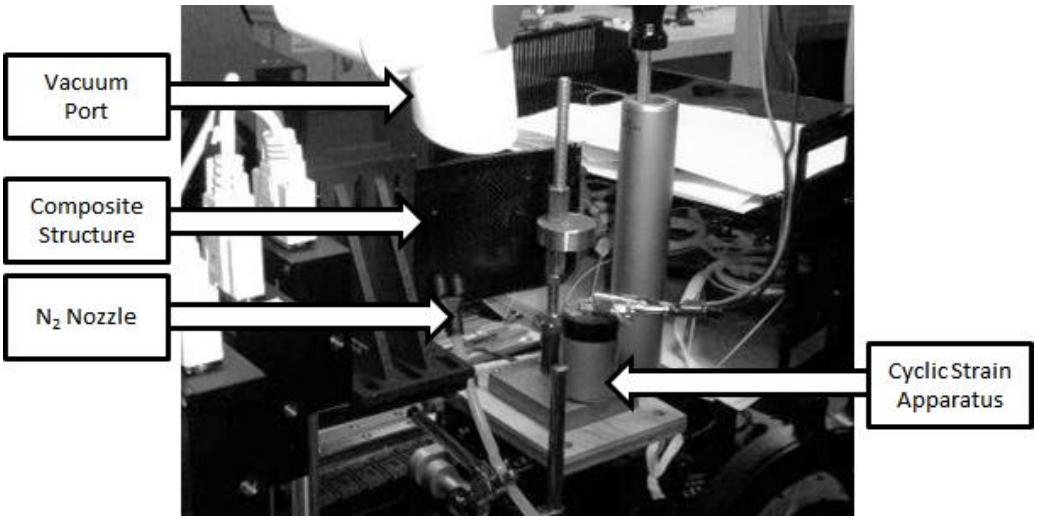

Figure 14: Complete test chamber setup for combined thermal and strain tests using a 25-Watt infrared laser. This figure shows the front face of the composite structure containing the 3x2x2 FBG array. This is the incident face for the infrared laser beam.

4.3 Infrared Laser Test Results

The front face sensor responses for lasing at target location 2 (from Figure 13) are presented in this section. For the test setup shown in Figure 14, the front face and the back face experienced cyclic tension and compression,

respectively. The FBG array between the composite plies on the strain-neutral axis experienced minimal strain due to bending. After reviewing the data, it was determined that the composite structure was too thin to effectively use the through-thickness isolation strategy; nearly identical thermal effects were present through the structure thickness, preventing detection of a thermal gradient on only one face. The through-thickness isolation strategy may be more effective with a thicker composite structure. For this architecture, although the thermal effects could not be easily isolated from the strain effects using the through-thickness FBG array, thermal effects were highly localized in-plane, as the results will show.

Figure 15 shows the combined strain and temperature responses of the FBGs on the front face. The 0.3 Hz cyclic loading caused the FBGs on the front face to oscillate between a negligible Bragg wavelength shift and a positive Bragg wavelength shift, as shown in Figure 15. At time 20 seconds, the infrared laser turned on, aimed 1.0 cm above the 1555 nm FBG. At time 40 seconds, the laser was turned off.

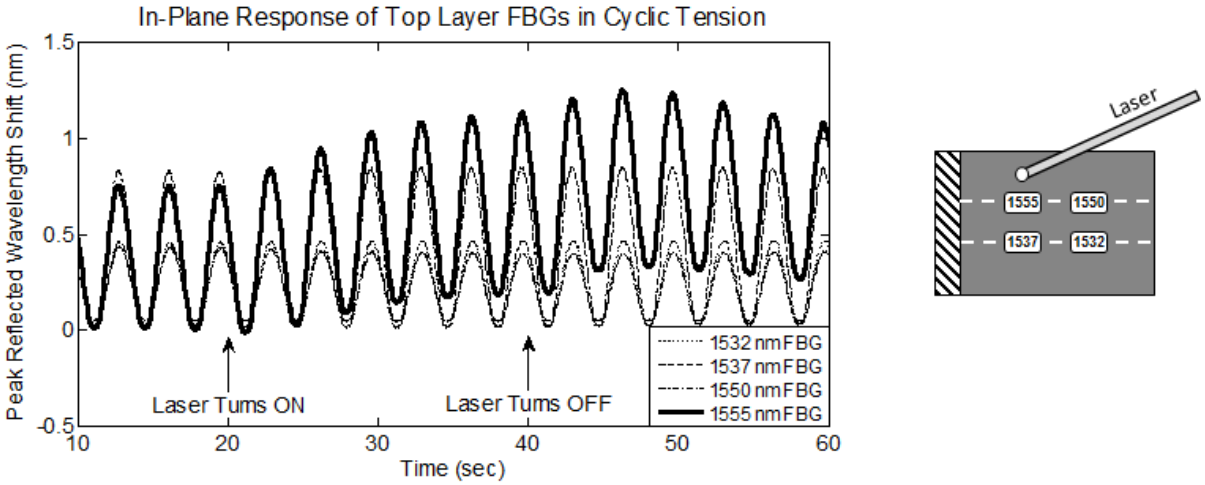

Figure 15: Front face in-plane response for four FBGs. Cyclic tension on this composite face induces the sinusoidal features seen in each trace. At 20 seconds, the infrared laser is turned on. At 40 seconds, the laser is turned off. Localized thermal effects are measured by the 1555 nm sensor. The diagram to the right shows the location of each of the sensors on the composite surface and the location of the target.

In Figure 15, two important initial observations can be made about the thermal response. First, a thermal gradient is observed only in the sensor response of the 1555 nm FBG, as expected based on the proximity of target location 2 to the 1555 nm FBG. Second, the thermal response of the 1555 nm FBG appears to be very consistent with earlier tests performed on a similar carbon/epoxy test structure that did not include strain effects.[5] Similar to those tests, although the maximum shift in the Bragg wavelength is delayed by more than 20 s after the laser is turned on, some heating is observed almost immediately, as shown in Figure 15 by an upshift in λ_B (in the solid curve) within seconds after the laser energy is applied. This is expected because of the higher thermal conductivity of the carbon epoxy/composite when compared to materials such as E-glass/epoxy composites, which demonstrate slower response times.

There is one additional observation based on the results in Figure 15. For the oscillating strain responses in Figure 15, there are two distinct amplitudes. The oscillations with the smaller amplitude shift (0.45 nm) occur in the 1550 nm and the 1532 nm FBGs. As shown in Figure 13, these gratings are embedded closest to the unclamped end of the structure, where the strain is applied. In contrast, the larger amplitude (0.7 nm) oscillations occur in the 1555 nm and the 1537 nm FBGs. These gratings are embedded farther from the mechanical load. This result is expected for a beam-like structure fixed at one end. Figure 16 illustrates a free-body diagram of this structure.

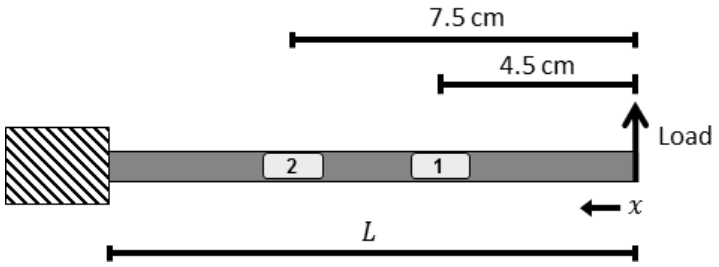

Figure 16: Free-body diagram for the 3x2x2 test array structure in Figure 13 under loading conditions (top view). Location 1 corresponds to the position of the 1550 and 1532 nm sensors. Location 2 is at the position of the 1555 and 1537 nm sensors.

With reference to Figure 16, the strain at distance x_i from the load is proportional to x_i, such that

$$\varepsilon_i \propto \frac{x_i}{L}, \tag{8}$$

where the dimension L is defined as the distance from the clamp to the load. To compare the relationship between sensor strain responses at locations 1 and 2, a strain compensation factor is defined as

$$K_i = \frac{\varepsilon_1}{\varepsilon_i} = \frac{x_1}{x_i}. \tag{9}$$

Solving Equation (9) at locations 1 and 2 with x_1 = 4.5 cm and x_2 = 7.5 cm gives strain compensation factors of K_1 = 1.00 and K_2 = 0.60. Graphically in Figure 15, this means that if the FBG responses from location 2 (for the 1555 nm and 1537 nm sensors) are scaled to 60% of their original value, the compensated strain responses will match at both locations. It is evident from Figure 15 that this is accurate. Strain compensation was a critical component in the data processing algorithm that was developed and will be discussed further below.

5. DATA PROCESSING ALGORITHM

There were two fundamental design requirements for the data processing algorithm that was developed to analyze the responses from the 3x2x2 sensor array. First, the algorithm must accurately detect localized thermal gradients with a high degree of probability. Second, the algorithm should be relatively fast, with a reasonably short execution time, allowing for repeated scans of the sensor array in real time. Ultimately, the specific software implementation that is needed to support each requirement depends on the specific design and application of the sensor array. As a proof-of-principle data processing demonstration, both design requirements are given equal importance in this research.

Figure 17 depicts the data processing algorithm using a block diagram. The data requires some initial preparation before processing with the thermal gradient detection algorithm. Each segment of this block diagram will be addressed below.

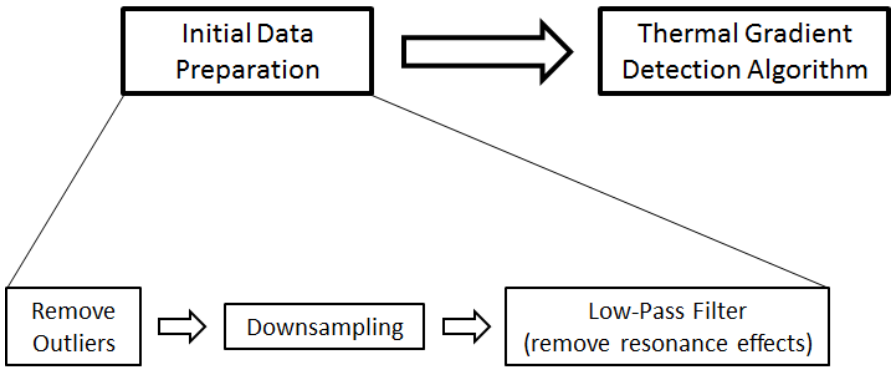

Figure 17: Block diagram overview of the data processing algorithm.

5.1 Initial Data Preparation

After the test data was collected by the SmartScan interrogator, it was imported into MATLAB® for initial processing. To account for any anomalous values collected by the interrogator, each of the data vectors recorded for the 12 FBGs in the 3x2x2 array are analyzed to detect unusual outliers in the data. Since the SmartScan interrogator repetitively records the Bragg wavelength of an FBG at a relatively high scan rate, an outlier is any shift in the Bragg wavelength from sample time t_{k-1} to time t_k that is unreasonably large. For the 500 Hz scan rate ($t_k - t_{k-1} = 2$ ms) used in this research, any Bragg wavelength jump of more than 2 nm was considered to be anomalous and was replaced with the previous valid Bragg wavelength. This is logical, given that the actual response time of an FBG temperature sensor is typically around 50 ms.[5]

Once outliers are removed, the data can be downsampled if desired to reduce the execution time of the algorithm. Downsampling is a process whereby every *n*th sample in the data vector is retained and all other data values are discarded. In effect, downsampling decreases the scan rate by a factor of *n*, thereby also reducing the stored data by a factor of *n*. This is common in signal processing and can be used if the scan rate (500 Hz in these tests) is larger than needed to capture the transient effects of temperature and strain. In the controlled laboratory environment of this research, all thermal and strain effects occurred at low frequencies (1-20 Hz), so downsampling from the 500 Hz scan rate was appropriate and reduced the algorithm execution time. In general, however, further testing would be required to assess if downsampling is appropriate for a given architecture and its anticipated operating environment.

Lastly, all data vectors were filtered using a zero-phase distortion low pass filter (LPF) to remove any strain responses resulting from vibrations at the natural resonance frequency of the structure. For the host structure of the 3x2x2 FBG array (with a length of 11.4 cm), the fundamental resonance occurred at 18.5 Hz when clamped on the end. To remove any noise in the data vector due to natural vibrations, the LPF was applied with a corner frequency below this frequency. Figure 18 is a graphical example of the effects of LPF filtering. In the figure, the original signal was generated by flicking the composite structure diagramed in Figure 16 every second or so with a finger, causing vibration in the composite at its natural resonant frequency. The LPF removes the vibrations due to the natural resonance while preserving the compression impulses (bold curve) due to flicking.

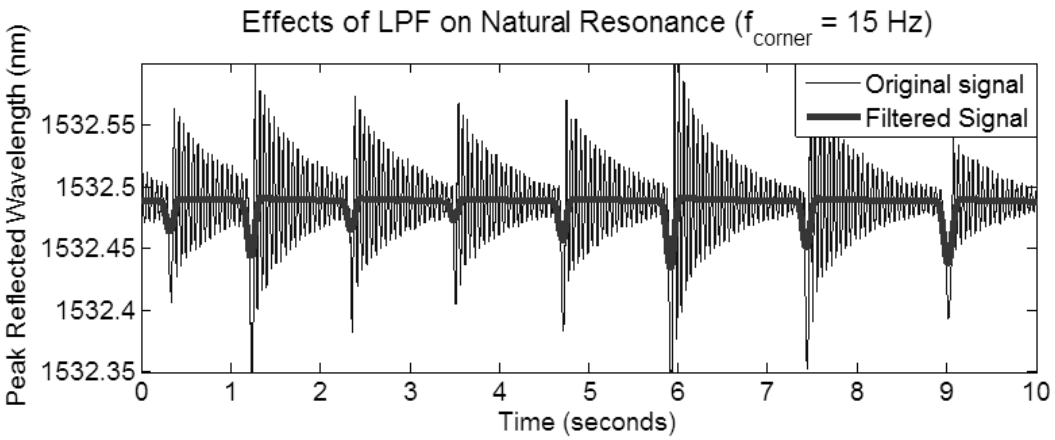

Figure 18: Effects of LPF on a signal containing a natural resonance frequency response at 18.5 Hz. The corner frequency of the LPF was 15 Hz—low enough to remove the 18.5 Hz resonance.

5.2 Thermal Gradient Detection

The thermal gradient detection algorithm relies on a statistical comparison of the FBG responses of all four gratings in each layer of the 3x2x2 array. Although the statistical analysis is repeated for each fiber layer (front face, middle, and back face), for simplicity, this discussion will describe the algorithm as it applies to a single layer.

First, the four FBG responses are time averaged over the scan time window, with the average wavelength shift represented as $\langle \Delta\lambda \rangle_{ti}$, where $i = 1,\ldots,4$. The appropriate strain compensation factor K_i is then applied, dependent on the sensor position x_i along the composite. The four sensor responses can then be characterized by their compensated mean values μ_i:

$$\mu_i = K_i \langle \Delta\lambda \rangle_{ti} \text{ , where } i = 1, \ldots, 4. \tag{9}$$

The standard deviation σ_4 of the four values of μ_i is given by

$$\sigma_4 = \sqrt{\frac{1}{4}\sum_{i=1}^{i=4}(\mu_i - \overline{\mu_i})^2}\,. \tag{10}$$

The parameter values μ_i and σ_4 are the fundamental statistical parameters describing the response of the four sensors at a given layer in the composite structure.

To determine if the statistical parameters indicate that a temperature shift has occurred, the largest (maximum) μ_i value is first replaced by the average of the remaining three μ_i values in order to eliminate any outliers in μ_i due to a thermal gradient. Based on the revised values of μ_i, the standard deviation $\sigma_{revised}$ is then recalculated. If the revised standard deviation is unchanged, such that $\sigma_{revised} \approx \sigma_4$, then no thermal gradient is likely present on the composite surface. However, if the ratio of these two standard deviations, given by

$$a = \frac{\sigma_4}{\sigma_{revised}}, \tag{11}$$

is large enough, a localized thermal gradient may be present. An empirically determined threshold value for a was chosen between 1.5 and 1.7. For values of a below the threshold, no localized thermal gradient is present. If a exceeds the threshold, then a thermal gradient is present.

Figure 19 depicts a graphical representation of the algorithm for the data presented in Figure 15. As shown on the left side of Figure 19, the original four values of μ_i and the corresponding standard deviation are calculated, resulting in σ_4 = 0.0421 nm. The maximum value of the four μ_i (associated with the FBG nearest to the laser target location) is replaced by the average of the remaining three values of μ_i. After removing the localized effect, associated with the 1555 nm FBG, the standard deviation drops appreciably to $\sigma_{revised}$ = 0.0110 nm. For the data in Figure 15, a = 0.0421nm/0.0110nm = 3.8177 > 1.7, indicating that the algorithm correctly detected the presence of a localized thermal gradient.

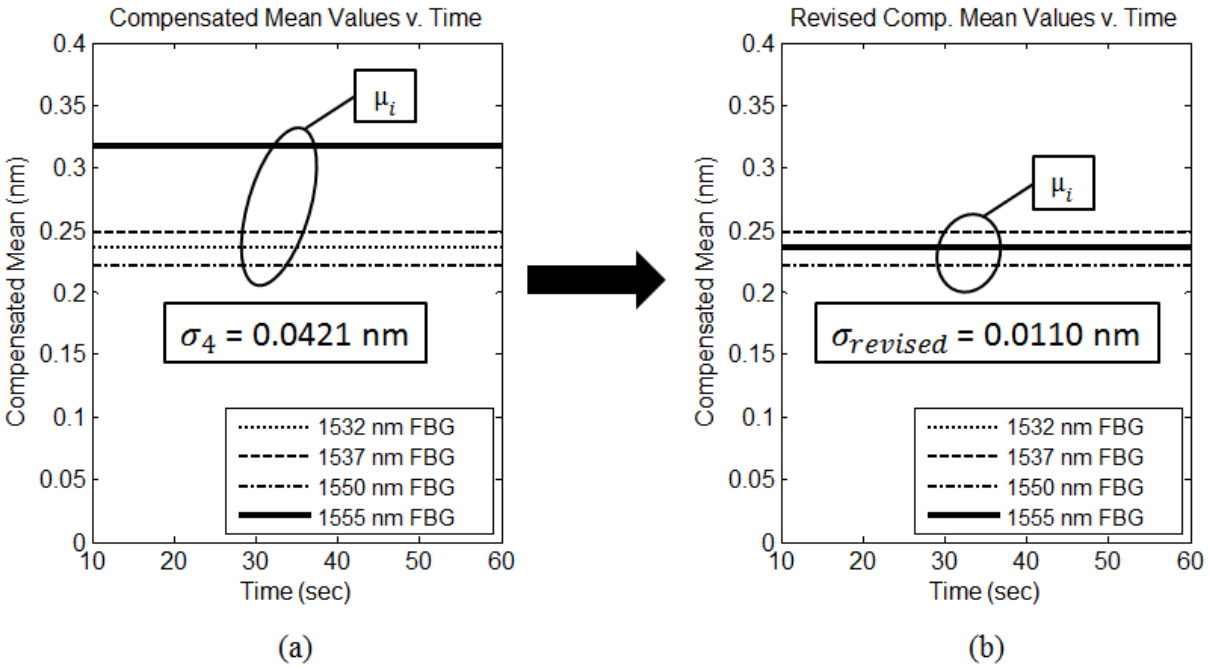

Figure 19: Graphical representation of the thermal detection algorithm. See Figure 15 for the original FBG responses. (a) The four μ_i values are plotted. (b) The maximum μ_i is replaced by the average of the remaining three μ_i's. The standard deviations of both sets of values are given in bold above.

This statistical approach is chosen instead of more sophisticated data processing techniques primarily for the sake of efficiency and as an initial proof-of-principle. Increasing the sophistication of the algorithm generally entails more data manipulation. As the array size is scaled up, the set of μ_i values per layer scales to i = 1, 2, …, n x m. It is clear that scaling up three-dimensional arrays quickly increases the processing time. Using easily calculated statistical parameters such as the average and standard deviation may save valuable execution time over alternative approaches.

5.3 Algorithm Results

The data processing algorithm written to process the data in Figure 15 requires four arguments. To filter the natural resonance of the structure, a corner frequency of 15 Hz is used. The data is downsampled by a factor of 10, reducing the effective sample rate form 500 Hz to 50 Hz. A standard deviation threshold of 1.7 is chosen to compare to the ratio a. Lastly, a strain compensation factor of K_2 = 4.5cm/7.5cm = 0.60 was used. Using these four parameters and the input data file, the MATLAB® script determines that a highly localized thermal gradient is present, as shown in Figure 20.

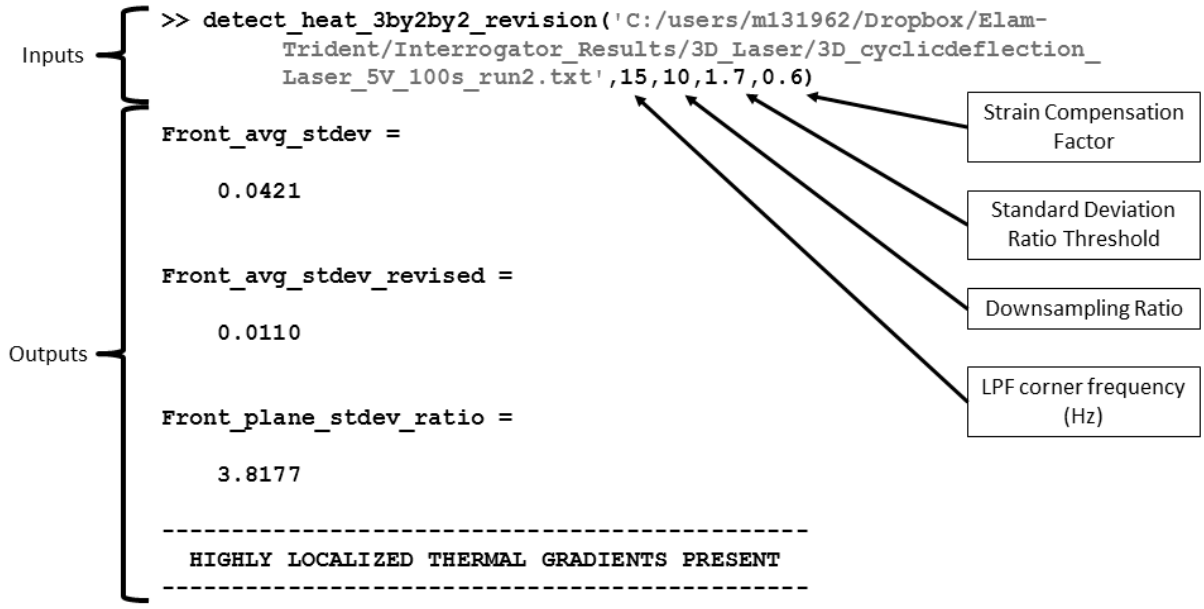

Figure 20: MATLAB® Command Window excerpt showing a function call to the algorithm named "detect_heat_3by2by2_revision". For these input arguments, the algorithm correctly determines that highly localized thermal gradients are present.

6. CONCLUSIONS

Several conclusions are evident. First and foremost, embedded fiber Bragg grating temperature sensors can be used to detect localized thermal gradients on the surface of a composite even in the presence of mechanical strain. The speed of detection remains to be determined, as it depends on numerous other factors, such as the thermal conductivity of the composite, the structural architecture, the spacing of the FBG sensors, and the execution time of the detection algorithm.

With regard to structural isolation, the through-thickness array remains promising for detecting localized thermal gradients in thick structures with sufficient thermal mass to prevent surface-layer thermal effects from penetrating quickly through the depth of the structure. The in-plane array is more appropriate for thin composite structures. Important parameters for the design of a real structure, such as the number and spacing of sensors throughout the array, the thickness of the composite, and the type of materials, depend on many factors. The specific application and the physical dimensions of the temperature gradient (i.e., spot size of the laser) must be known before a real "smart" structure can be designed and implemented.

For the data processing algorithm, a statistical analysis of the data collected from the 3x2x2 FBG array was effective and efficient. Depending on the operating environment of the embedded FBG array, various data preparation techniques may be needed before the thermal detection algorithm is applied. Examples include downsampling and filtering of natural vibration resonances using a zero-phase distortion LPF. For a real-time isolation strategy, the thermal detection algorithm may require the use of running averages with greater precision and accuracy to rapidly detect the presence of a thermal gradient on the surface of the composite. As before, the specific application of the sensor array will impact the design choices required to appropriately tailor this proof-of-principle strategy.

7. FUTURE WORK

Significant research is still needed to effectively use embedded FBG sensor technology in composite structures. Given the breadth of possible applications for SHM in composites, more focused research is needed to characterize both temperature and strain effects in composites. To better understand the thermal effects, the interaction between convection and conduction as heat transfer mechanisms bust be analyzed to determine their influence on the sensor

network design. Additionally, further development of the data processing algorithm is necessary, as it could assist in determining the severity and spatial location (in three dimensions) of a thermal gradient. This would require a more detailed analysis of the response data from an *n* x *m* array of sensors through the thickness of a structure. Such information is important in order to model heat transfer in composite materials.

A more rigorous analysis of complex strain effects must also be considered. In this research, strain was applied in a deterministic, oscillatory manner; unfortunately practical applications of such sensor arrays will not likely experience such controlled strain profiles. A more stochastic application of strain in time should be considered, and the accompanying data processing features should be modified accordingly. This will require emphasis on developing a real-time data processing scheme. In this research, data was collected during each test and processed later. Any practical application of a data processing algorithm must necessarily be able to process incoming data as quickly as it is gathered. As such, the execution time of this algorithm must be reduced to ensure detection in a minimal amount of time. It is clear that there is a significant opportunity and need for further research in the field of embedded FBG arrays in composite materials.

REFERENCES

[1] Kersey, A. D., Davis, M. A., Patrick, H. J., LeBlanc, M., Koo, K. P., Askins, C. G., Putnum, M. A., and Friebele, E. J., "Fiber Grating Sensors," Journal of Lightwave Technology 15(8), 1442-1463 (1997).

[2] Wu, M. C., Winfree, W. P., and Allison, S. G., "Fiber optic thermal health monitoring of aerospace structures and materials," Proc. SPIE 7294 (2009).

[3] Propst, A., Peters, K., Zikry, M. A., Schultz, S., Kunzler, W., Zhu, Z., Wirthlin, M., and Selfridge, R., "Assessment of damage in composite laminates through dynamic, full-spectral interrogation of fiber Bragg grating sensors," Smart Materials and Structures 19, 1-11 (2010).

[4] Epaarachchi, J. A., Canning, J., and Stevenson, M., "The response of embedded NIR (830nm) fiber Bragg grating sensors in glass fiber composites under fatigue loading," Journal of Composite Materials 44(7), 809-819 (2010).

[5] Jenkins, B., Joyce, P., Mechtel, D., Milden, K., Elam, K., and Watkins, J., "Highly-localized thermal response measurements in composites using embedded fiber Bragg grating temperature sensors," Proc. SPIE 8693 (2013).

APPENDIX A: DATA PROCESSING ALGORITHM

Filename: "detect_heat_3by2by2_revision.m"

```
% Analyzes data collected from the SmartScan interrogator from the
% 3x2x2 array.  Primary approach will be an in-plane comparison of
% neighboring gratings.
%
% Input arguments:
% 1.) The filename of a single .txt file containing 13
% columns of data.  The first, left-most column is a time vector.
% The remaining 12 columns contain the data from the sensors.
% 2.) The LPF corner frequency desired for low-pass filtering
% 3.) Downsample ratio.  If sampling rate is high, downsampling can
% boost speed of filtering operations.
% 4.) Standard Deviation ratio threshold.  A thresholding parameter to
% govern decision-making of whether localized thermal gradients exist
% in-plane.  Recommended value between 1.4 and 1.7.
% 5.) Strain Compensation Factor.  Compensates for linear increase in
% strain for a clamped specimen (0.6 for 3D sample).
%
% Fibers in each plane:
% Fibers 1 & 4: Top/Front plane
% Fibers 2 & 5: Middle plane
% Fibers 3 & 6: Back plane
%
% Grating arrangement (looking at side labeled "TOP"):
%                    -----------------------------------------
% Top (4,5,6):       |  <Grating D>              <Grating C>  |
%                    |                                        |
%                    |                                        |
% Bottom (1,2,3):    |  <Grating B>              <Grating A>  |
%                    -----------------------------------------
%
% Signal Processing Scheme:
% 1. Load all data appropriately
% 2. Downsample data as desired
% 3. Filter all data to remove natural vibrational resonance frequencies
% 4. Determine the presence of a thermal gradient
% 5. Return results

%-------------------------------------------------------------------------

function
detect_heat_3by2by2_revision(filename,f_LPF_corner,downsample_ratio,...
    stdev_ratio_thresh,SCF)

% clc

local_hit = 0; % establishes a flag variable for detecting localized heat
               % present in the composite
Front_plane_local_hit = 0;
Middle_plane_local_hit = 0;
Back_plane_local_hit = 0;
```

```
%-------------------------------------------------------------------------

% 1. Load data using importdata function
mystruct = importdata(filename,'\t',5);
mydata = mystruct.data;
time = mydata(:,1);

% Front plane:
peak_4D = mydata(:,2);
peak_4C = mydata(:,3);
peak_1B = mydata(:,4);
peak_1A = mydata(:,5);
% Middle plane:
peak_5D = mydata(:,6);
peak_5C = mydata(:,7);
peak_2B = mydata(:,8);
peak_2A = mydata(:,9);
% Back plane:
peak_6D = mydata(:,10);
peak_6C = mydata(:,11);
peak_3B = mydata(:,12);
peak_3A = mydata(:,13);

% Declare nominal wavelengths for each grating
% Nominal Wavelengths
nom_1A = 1532.54;
nom_1B = 1537.44;
nom_4C = 1550.30;
nom_4D = 1555.37;
nom_2A = 1532.44;
nom_2B = 1537.38;
nom_5C = 1550.29;
nom_5D = 1555.34;
nom_3A = 1532.19;
nom_3B = 1536.96;
nom_6C = 1550.27;
nom_6D = 1555.05;

% Scrub channel 3 for outlier entries
temp = nom_3A;
for k=2:length(peak_3A)
    if (abs(peak_3A(k) - peak_3A(k-1)) > 2)
        peak_3A(k) = temp; % repeat last valid data point
    else
        temp = peak_3A(k);
    end
end

temp = nom_3B;
for k=2:length(peak_3B)
    if (abs(peak_3B(k) - peak_3B(k-1)) > 2)
        peak_3B(k) = temp; % repeat last valid data point
    else
```

```
        temp = peak_3B(k);
    end
end

temp = nom_6C;
for k=2:length(peak_6C)
    if (abs(peak_6C(k) - peak_6C(k-1)) > 2)
        peak_6C(k) = temp; % repeat last valid data point
    else
        temp = peak_6C(k);
    end
end

temp = nom_6D;
for k=2:length(peak_6D)
    if (abs(peak_6D(k) - peak_6D(k-1)) > 2)
        peak_6D(k) = temp; % repeat last valid data point
    else
        temp = peak_6D(k);
    end
end

%-------------------------------------------------------------------------

% 2. Downsampling (as desired).  Determine time resolution,
% sampling frequency
t_res_hardware = (time(length(time)) - time(1)) / (length(time) - 1);
fs_hardware = 1/t_res_hardware;

if (downsample_ratio > 1)
    time = downsample(time,downsample_ratio);
    peak_4D = downsample(peak_4D,downsample_ratio);
    peak_4C = downsample(peak_4C,downsample_ratio);
    peak_1B = downsample(peak_1B,downsample_ratio);
    peak_1A = downsample(peak_1A,downsample_ratio);
    peak_5D = downsample(peak_5D,downsample_ratio);
    peak_5C = downsample(peak_5C,downsample_ratio);
    peak_2B = downsample(peak_2B,downsample_ratio);
    peak_2A = downsample(peak_2A,downsample_ratio);
    peak_6D = downsample(peak_6D,downsample_ratio);
    peak_6C = downsample(peak_6C,downsample_ratio);
    peak_3B = downsample(peak_3B,downsample_ratio);
    peak_3A = downsample(peak_3A,downsample_ratio);
    fs = fs_hardware/downsample_ratio;
else
    fs = fs_hardware;
end

%-------------------------------------------------------------------------

% 3. Filter all signals to remove natural frequency responses due to
% vibration, etc.  Natural resonance frequency of panel clamped on
% one end for ~1 inch, leaving a ~5.5 inch span of CF two-ply
% composite to vibrate, is roughly 18.5 Hz.  Use a low-pass filter with
```

```
% corner frequency f_LPF_corner to cut off all high frequency content
% (including natural resonance effects).
filt_4D = ElamSimpleLPF(peak_4D,fs,f_LPF_corner);
filt_4C = ElamSimpleLPF(peak_4C,fs,f_LPF_corner);
filt_1B = ElamSimpleLPF(peak_1B,fs,f_LPF_corner);
filt_1A = ElamSimpleLPF(peak_1A,fs,f_LPF_corner);
filt_5D = ElamSimpleLPF(peak_5D,fs,f_LPF_corner);
filt_5C = ElamSimpleLPF(peak_5C,fs,f_LPF_corner);
filt_2B = ElamSimpleLPF(peak_2B,fs,f_LPF_corner);
filt_2A = ElamSimpleLPF(peak_2A,fs,f_LPF_corner);
filt_6D = ElamSimpleLPF(peak_6D,fs,f_LPF_corner);
filt_6C = ElamSimpleLPF(peak_6C,fs,f_LPF_corner);
filt_3B = ElamSimpleLPF(peak_3B,fs,f_LPF_corner);
filt_3A = ElamSimpleLPF(peak_3A,fs,f_LPF_corner);

%--------------------------------------------------------------------------

% 4. Locate affected Grating set

% ---------------------
% Front Plane:
% Create vector with each gating in plane's average peak wavelength, but
% subtract out each grating's nominal wavelength (gives average wavelenth
% shift over entire time period)
Front_plane = [ (mean(filt_4D)-nom_4D) (mean(filt_4C)-nom_4C)...
    (mean(filt_1B)-nom_1B) (mean(filt_1A)-nom_1A) ]
% Find standard deviation of these averages
Weighting = [SCF, 1, SCF, 1];
Front_avg_stdev = std(Weighting .* Front_plane)

% Remove largest deviator from vector and recalculate standard
% deviation
updated_Front_plane = Front_plane;
[m,i] = max(Weighting .* updated_Front_plane);
updated_Front_plane(i) = 0;
updated_Front_plane(i) = sum(Weighting .* updated_Front_plane/3)
Weighting(i) = 1;
updated_Front_avg_stdev = std(Weighting .* updated_Front_plane)

% Determine ratio of previous stdev to recalculated stdev.  If the ratio
% exceeds stdev_threshold, then consider there to be localized thermal
% effects in this plane
Front_plane_stdev_ratio = Front_avg_stdev / updated_Front_avg_stdev
if (Front_plane_stdev_ratio > stdev_ratio_thresh)
    Front_plane_local_hit = 1;
end

% ---------------------

% Middle Plane:
Middle_plane = [ (mean(filt_5D)-nom_5D) (mean(filt_5C)-nom_5C)...
    (mean(filt_2B)-nom_2B) (mean(filt_2A)-nom_2A) ];
% Find standard deviation of these averages
Weighting = [SCF, 1, SCF, 1];
```

```
Middle_avg_stdev = std(Weighting .* Middle_plane);

% Remove largest deviator from vector and recalculate standard
% deviation
updated_Middle_plane = Middle_plane;
[m,i] = max(Weighting .* updated_Middle_plane);
updated_Middle_plane(i) = 0;
updated_Middle_plane(i) = sum(Weighting .* updated_Middle_plane/3);
Weighting(i) = 1;
updated_Middle_avg_stdev = std(Weighting .* updated_Middle_plane);

% Determine ratio of previous stdev to recalculated stdev.  If the ratio
% exceeds stdev_threshold, then consider there to be localized thermal
% effects in this plane
Middle_plane_stdev_ratio = Middle_avg_stdev / updated_Middle_avg_stdev
if (Middle_plane_stdev_ratio > stdev_ratio_thresh)
    Middle_plane_local_hit = 1;
end

% ---------------------

% Back Plane:
Back_plane = [ (mean(filt_6D)-nom_6D) (mean(filt_6C)-nom_6C)...
    (mean(filt_3B)-nom_3B) (mean(filt_3A)-nom_3A) ];
% Find standard deviation of these averages
Weighting = [SCF, 1, SCF, 1];
Back_avg_stdev = std(Weighting .* Back_plane);

% Remove largest deviator from vector and recalculate standard
% deviation
updated_Back_plane = Back_plane;
[m,i] = max(Weighting .* updated_Back_plane);
updated_Back_plane(i) = 0;
updated_Back_plane(i) = sum(Weighting .* updated_Back_plane/3);
Weighting(i) = 1;
updated_Back_avg_stdev = std(Weighting .* updated_Back_plane);

% Determine ratio of previous stdev to recalculated stdev.  If the ratio
% exceeds stdev_threshold, then consider there to be localized thermal
% effects in this plane
Back_plane_stdev_ratio = Back_avg_stdev / updated_Back_avg_stdev
if (Back_plane_stdev_ratio > stdev_ratio_thresh)
    Back_plane_local_hit = 1;
end


%-------------------------------------------------------------------------

% 5. Make decision and return results

% Decision:
if ( (Front_plane_local_hit == 1) && (Middle_plane_local_hit == 1) ...
        && (Back_plane_local_hit == 1) )
```

```
    local_hit = 1;
end % recall local_hit is set to 0 by default

if (local_hit == 1)
    disp('-----------------------------------------------');
    disp('  HIGHLY LOCALIZED THERMAL GRADIENTS PRESENT');
    disp('-----------------------------------------------');
    %return;
else
    disp('-------------------------------------------------');
    disp('  NO highly localized thermal gradients present');
    disp('-------------------------------------------------');
    %return;
end
```

Filename: "ElamSimpleLPF.m"

```
% Applies a low pass filter to an input signal with corner frequency
% fc in Hz (greater than ~3 Hz).  The sampling frequency, fs, is also a
% required input.  Returns the filtered signal in vector form.

function filt = ElamSimpleLPF(input, fs, fc)

input_mean = mean(input); % record mean value
h = fdesign.lowpass(0.00005,fc*2/fs,1,50); % normalized frequencies
d = design(h,'equiripple');
filt = filtfilt(d.Numerator,1,input); % apply filter
filt = filt * input_mean/mean(filt);
            % recenter around the mean value of input signal
return
```

APPENDIX B: PROCEDURE TO EMBED OPTICAL FIBERS IN COMPOSITES

The procedure used in this research to embed optical sensor fibers in composite structures is detailed below. A traditional composite layup procedure was modified to account for two unique challenges regarding optical fibers. First, the procedure required precision and skill when handling the bare optical fibers (~150 μm in diameter). Second, both ends of the sensor fibers extended out from the sides of the composite structure, as shown in Figure 7. The protruding glass was brittle and limited the options available to cure the composite after the layup.

It is strongly recommended that the following procedure be tested prior to embedding the actual sensor fibers. Much less expensive conventional optical fiber pigtails (containing no FBGs) should be embedded in a sample composite structure to gain proficiency in handling fibers during the procedure. Then, after the process is mastered, the significantly more expensive FBG sensor fibers may be embedded in the structure.

B.1 Fiber Termination Labels

To begin, the precise location of each FBG in each fiber was determined using a heat gun. The fiber was slowly moved from side to side in front of the heat gun and the real-time interrogator response was simultaneously monitored. When one of the two FBGs in the fiber responded to the heat on the interrogator, the corresponding fiber termination was labeled with a letter, as shown in Figure 21. "A" corresponded to the 1532 nm FBG, "B" corresponded to the 1537 nm FBG, etc. Labeling each fiber termination ensured that the FBGs would be oriented properly when embedded. A black marker was used to place identification markings on each optical fiber between each termination and each FBG. The markings were at precise locations equidistant from the outer end of each FBG and outside the expected boundary of the composite material. In this manner, the sensor positions can easily be located after embedding them in the composite.

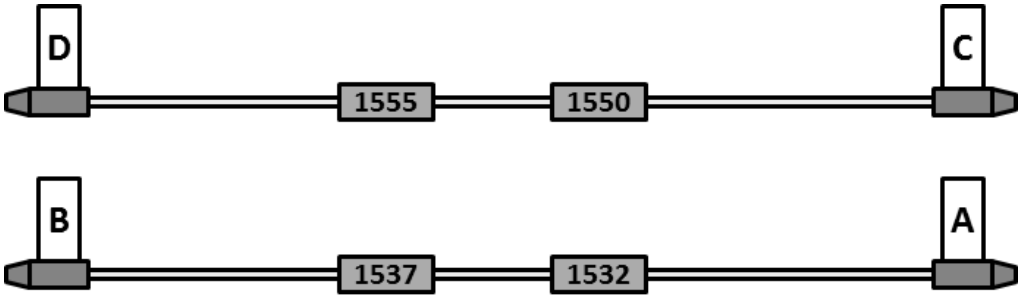

Figure 21: Fiber termination labels. The appropriate letter (for each Bragg wavelength) was written on a piece of tape around the nearest fiber termination. The A/B fibers contained the 1532 nm and 1537 nm FBGs. The C/D fibers contained the 1550 nm and 1555 nm FBGs.

The optical fibers used in this research were 3 meters in length. With roughly 1.5 meters of excess glass fiber on either end of the FBG sensors (located in the middle of the fiber), special care was taken to organize and protect the numerous bare optical fibers used in this array. In general, it was easier to handle the excess optical fiber when it was gently coiled. A conventional paper tray was useful to separate and sort the various coils of fiber ends, as the photograph in Figure 22 depicts.

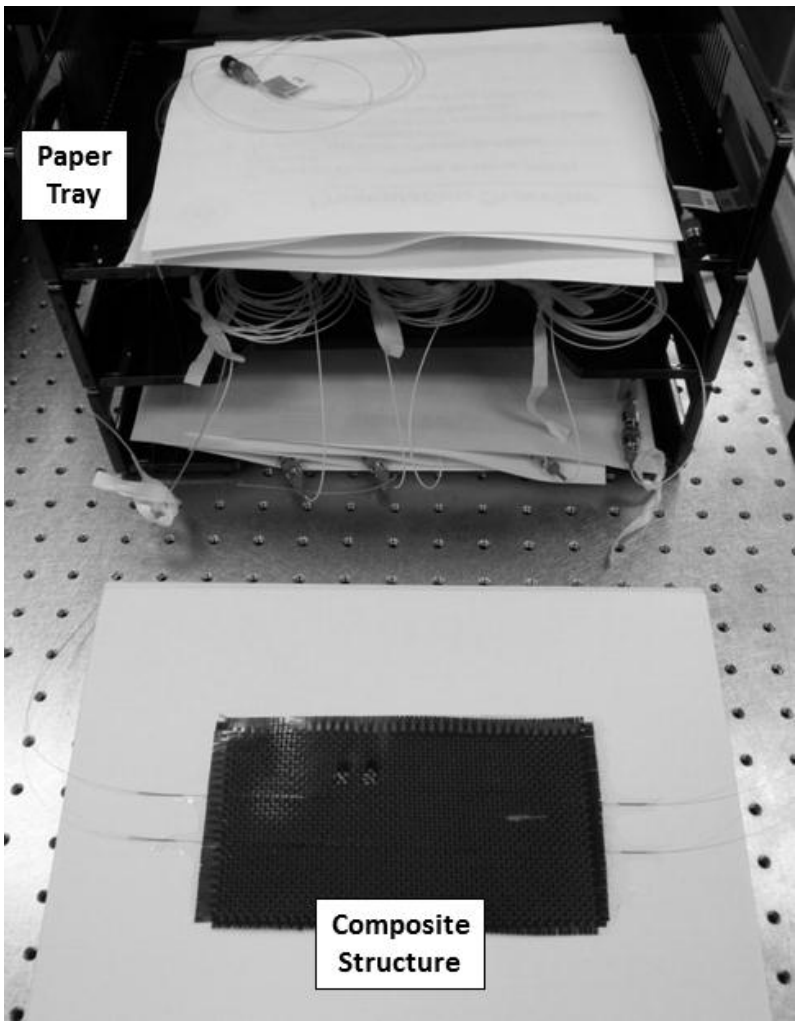

Figure 22: A conventional paper tray is used to sort the individually coiled optical fibers. Within a given tray, single sheets of paper were used to separate fiber coils. In the photograph, the middle tray held coiled fibers associated with the WDM devices diagramed in Figure 8.

B.2 Composite Layup

The composite materials for the layup procedure were then prepared. First, the six sensor fibers of the 3x2x2 array were laid out in a parallel fashion. Each adjacent fiber alternated between A/B and C/D fibers. Two 3.5 in. x 6.5 in. pieces of Fibre Glast 530-C 3K Plain Weave Carbon Fiber fabric were cut from a large roll. Also, West System® 105 Epoxy Resin and West System® 206 Slow Hardener were mixed (5 parts resin to 1 part hardener by volume) to create the polymer base of the composite structure.

To provide a non-stick surface for work, a 15”x15” piece of KM 1300 bagging material was taped to the work table. Fibers 3 and 6 were laid in parallel atop the bagging material and taped at the ends. Together, these two fibers constituted the bottom layer of the 3x2x2 sensor array. This layup setup is shown in Figure 23.

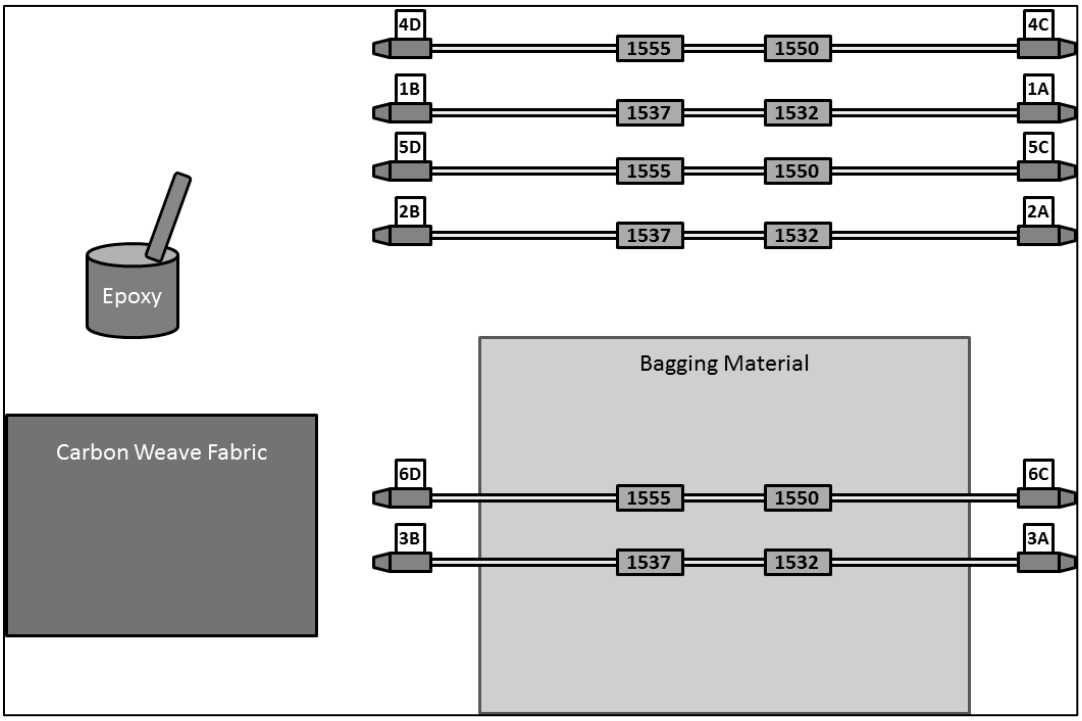

Figure 23: Composite layup setup. The sensor fibers are labeled and prepared for the embedding process. The bottom layer of the 3x2x2 FBG array (Fibers 3 and 6) are in place. Figure not to scale.

Next, the first ply of carbon fabric was centered atop the FBGs of Fibers 3 and 6. The fabric was then coated to saturation with epoxy resin; a tongue depressor was used to spread the epoxy over the surface. The adhesive properties of the epoxy resin alone kept the carbon fiber fabric in place. It was not necessary to apply epoxy resin to the optical fibers; the curing process described below ensured that they bonded well to the carbon fiber fabric. The middle layer of the 3x2x2 array (Fibers 2 and 5 in Figure 24) was then placed atop the first carbon ply, as shown in Figure 24. The fibers were taped at the ends to the work table, fixing them in place for the embedding process.

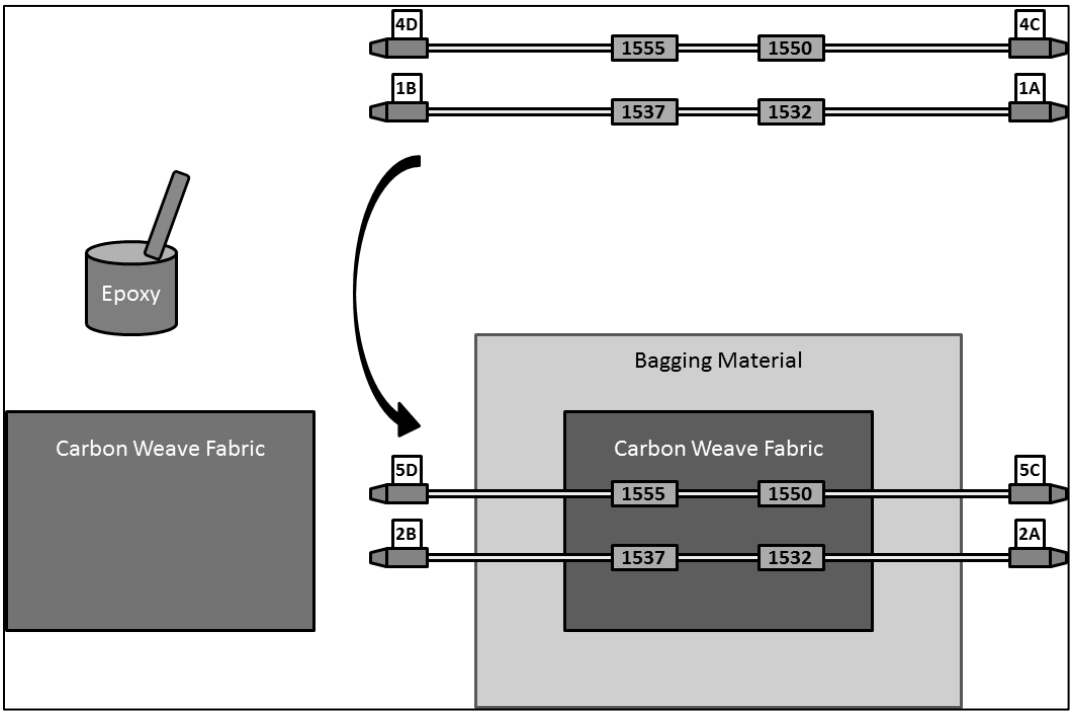

Figure 24: First carbon ply and the middle layer of FBG sensors (Fibers 2 and 5) put in place.

The second carbon ply was then placed atop the middle layer of FBGs. Epoxy was then applied to the fabric, as before. Then, the top layer of the 3x2x2 array (Fibers 1 and 4 in Figure 25) was moved atop the second carbon ply, as shown in Figure 25.

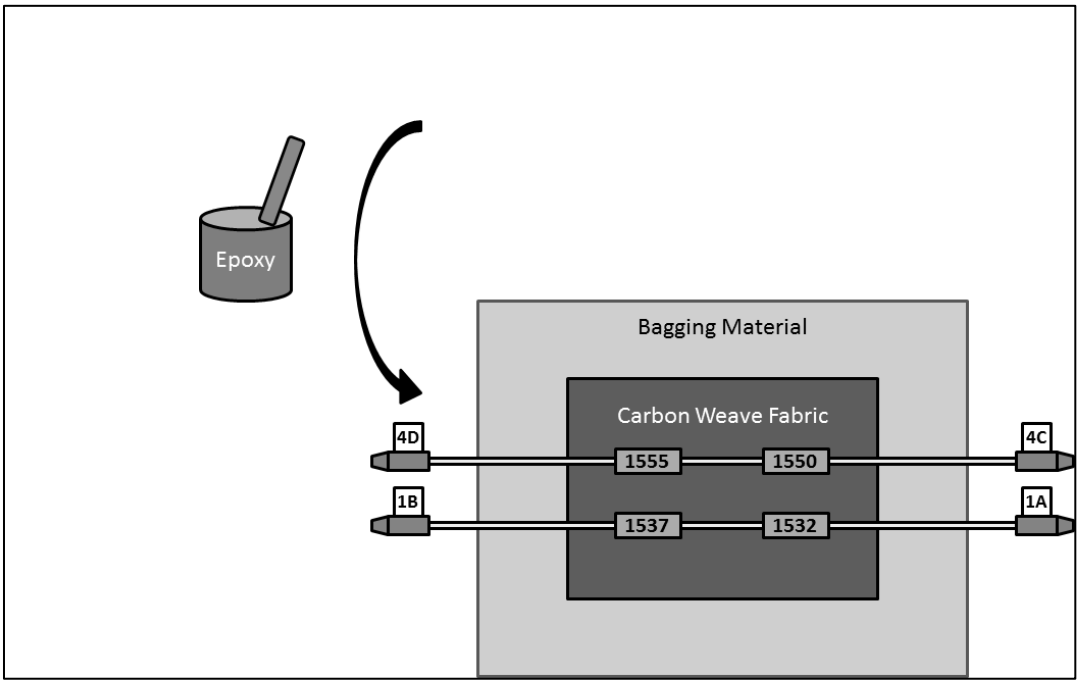

Figure 25: Second carbon ply and the top layer of FBG sensors (Fibers 1 and 4) in put in place.

B.3 Curing Process

With the FBG sensor array embedded in the composite layup, the epoxy resin required time to cure. To aid the curing process, a vacuum bag was created using the bagging material; the partial vacuum pressure removes air bubbles lodged in the layup materials. A line of vacuum sealant tape was placed around the perimeter of the bagging material sheet, allowing for an air-tight seal, even overtop the protruding fibers. A second sheet of bagging material (15"x15") was then cut, placed atop the layup, and sealed against the sealant tape to create the vacuum bag. A vacuum pump was connected to the bag to apply the vacuum condition. Unfortunately, a pressure gauge was not available to monitor the vacuum pressure achieved inside the bag. Figure 26 shows the final setup for the curing process.

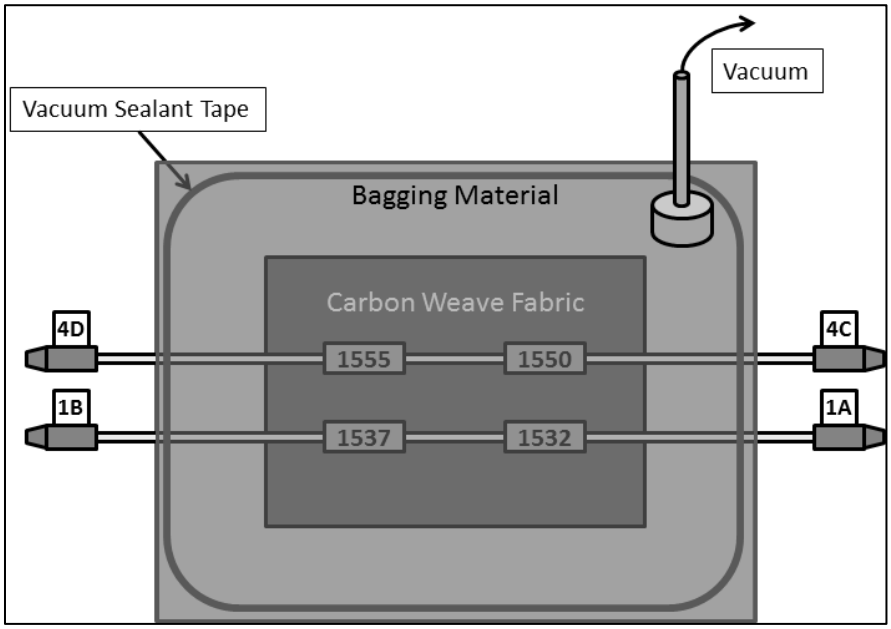

Figure 26: Final composite curing setup. The bagging material and sealant tape are used to create an air-tight bag enclosing the composite structure. The vacuum pump created a partial vacuum within the bag.

To ensure the composite cured properly, additional external pressure was required. The industrial-strength presses available during this research were too strong for this sensitive procedure; even at the lowest pressure settings, the press would crush the fragile optical fibers. Therefore, the additional pressure needed for the curing process was achieved using external weight. To protect the fibers in the layup, a thin piece of foam was laid atop the composite layup. Next, a caul plate was used to evenly distribute the additional pressure across the composite surface. Lastly, weights were stacked atop the caul plate to apply an additional 2 psi of external pressure (roughly 50 lbs. distributed over the 23 in^2 surface area of the composite structure). A vertical cross-section of this setup is given in Figure 27.

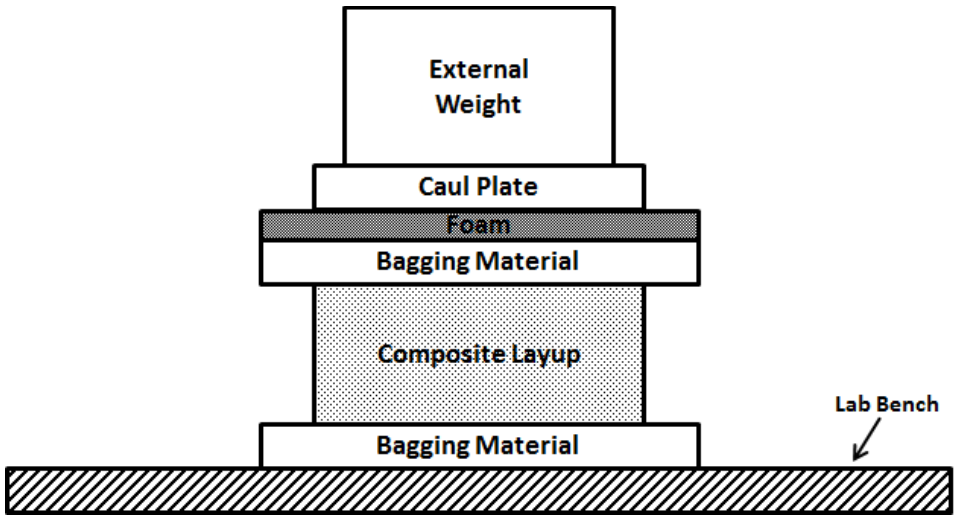

Figure 27: Vertical cross-section of the setup for curing the composite structure under external pressure.

The composite layup was allowed to cure overnight (~12 hours) at room temperature (20°C). After the epoxy had completely hardened, the vacuum pump was removed and the vacuum bag was cut away. The final product was a 3x2x2 FBG array embedded in a two-ply carbon/epoxy composite structure, as photographed in Figure 28.

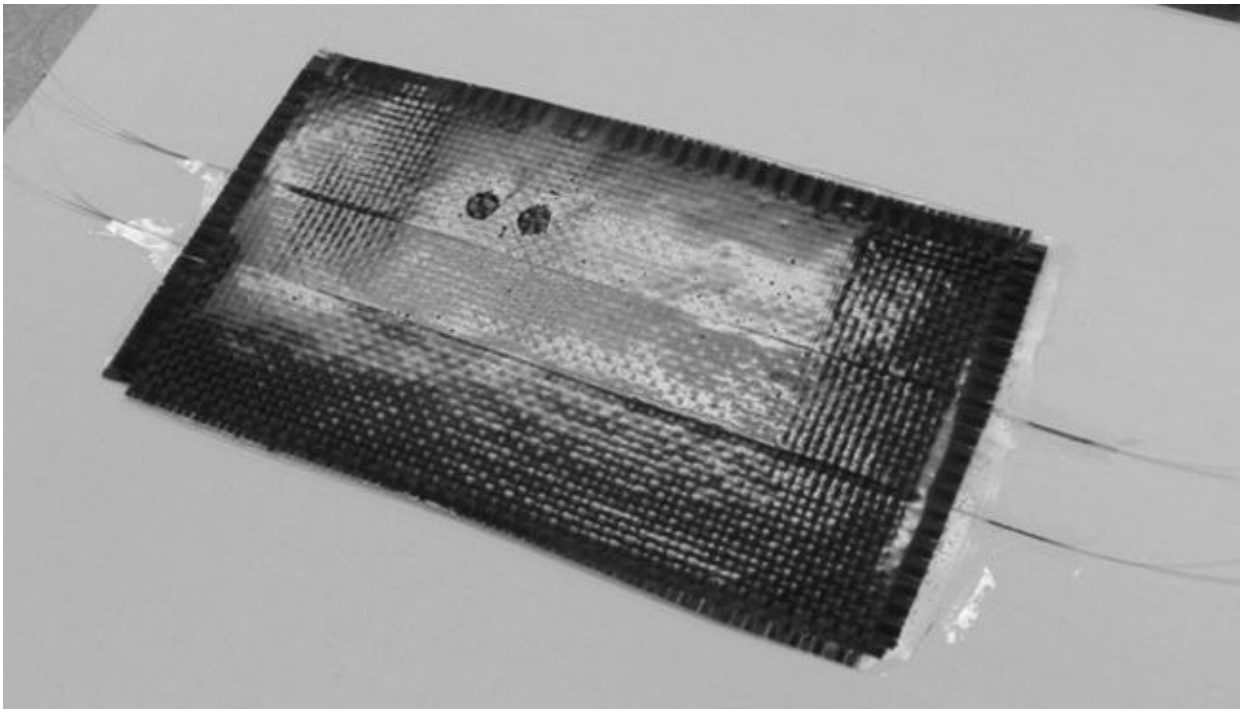

Figure 28: A 3x2x2 FBG array embedded in a two-ply carbon/epoxy composite. The six optical fibers are shown protruding out each end of the composite structure. The two circular flaws on the composite surface are the result of the later infrared laser testing and are not associated with this embedding procedure.